BIOCHEMISTRY
including biophysical chemistry & molecular biology

Current Topic

pubs.acs.org/biochemistry

Connecting Protein Conformational Dynamics with Catalytic Function As Illustrated in Dihydrofolate Reductase

Yao Fan, Alessandro Cembran, Shuhua Ma,[†] and Jiali Gao*

Department of Chemistry, Digital Technology Center, and Supercomputing Institute, University of Minnesota, 207 Pleasant Street Southeast, Minneapolis, Minnesota 55455, United States

Supporting Information

ABSTRACT: Combined quantum mechanics/molecular mechanics molecular dynamics simulations reveal that the M20 loop conformational dynamics of dihydrofolate reductase (DHFR) is severely restricted at the transition state of the hydride transfer as a result of the M42W/G121V double mutation. Consequently, the double-mutant enzyme has a reduced entropy of activation, i.e., increased entropic barrier, and altered temperature dependence of kinetic isotope effects in comparison with those of wild-type DHFR. Interestingly, in both wild-type DHFR and the double mutant, the average donor−acceptor distances are essentially the same in the Michaelis complex state (∼3.5 Å) and the transition state (2.7 Å). It was found that an additional hydrogen bond is formed to stabilize the M20 loop in the closed conformation in the M42W/G121V double mutant. The computational results reflect a similar aim designed to knock out precisely the dynamic flexibility of the M20 loop in a different double mutant, N23PP/S148A.

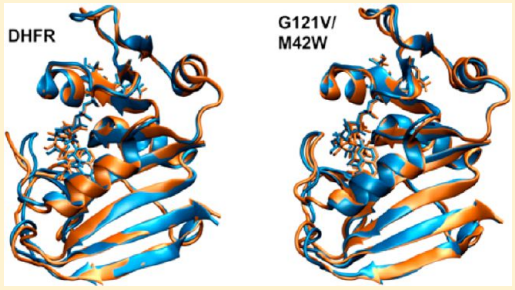

Protein dynamics are essential to the catalytic function of enzymes,[1−3] which range from femtosecond promoting vibrations and picosecond−nanosecond local fluctuations to millisecond and second conformational motions. The question, however, is the precise mechanism by which large-scale protein motions and fast, local dynamic fluctuations are connected to the chemical step to lower the free energy barrier.[4,5] Mutations distant from the active site, which do not show noticeable structural variations in enzyme−inhibitor complexes, provided indirect evidence, suggesting that altered protein motions may affect the reaction rate and transition state stabilization.[6−10] The effects are reflected in the observed kinetic data, including kinetic isotope effects (KIEs) and activation parameters.[11] Recently, the role of conformational dynamics in the chemical step of *Escherichia coli* dihydrofolate reductase (DHFR) was directly probed experimentally by mutations designed to block dynamic fluctuations of the M20 loop,[12,13] which has previously been shown to be critical to the enzymatic function.[6,14] It was concluded that the decreased rate of hydride transfer in the "dynamic knockout" mutants is due to impaired flexibility on the millisecond time scale,[12] but a different conclusion was drawn about the same system from measurements of KIEs.[13]

In this Current Topic, we focus on a specific study of the hydride transfer in *E. coli* dihydrofolate reductase (DHFR) and the M42W/G121V double mutant (Figure 1) to illustrate the procedure and analyses used in computer simulations to understand the role of protein conformational dynamics in the catalyzed reaction. The methods used and the principles that emerged from this specific investigation are likely to be generally applicable to other enzymes. DHFR is a relatively small, flexible protein that catalyzes the nicotinamide adenine dinucleotide phosphate (NADPH)-dependent reduction of 7,8-dihydrofolate to 5,6,7,8-tetrahydrofolate.[6,14,15] The catalytic mechanism of DHFR has been extensively studied, although we cannot afford to provide a thorough review of the large body of literature. NMR relaxation experiments established that conformational changes in flexible loops spread out of the protein play a critical role in modulating ligand specificity and catalytic turnover.[6,12,15−17] Furthermore, single and double mutations at the M42 and G121 sites as well as other locations that are remote from the catalytic center can nevertheless produce profound, nonadditive effects on

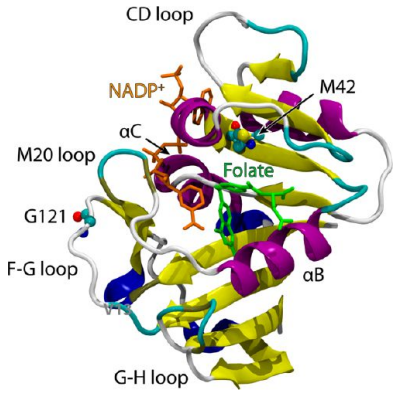

Figure 1. X-ray structure of the ternary complex of *E. coli* dihydrofolate reductase, folate substrate, and NADP+ cofactor (Protein Data Bank entry 1RX2). The secondary structure and loop nomenclature are indicated.

Received: November 20, 2012
Revised: January 4, 2013
Published: January 8, 2013

reaction rate, activation parameters, and the temperature dependence of KIEs.[13,18−26] Computational studies helped identify networks of interatomic distance variations along the reaction coordinate, and distal mutations can induce structural perturbations that alter these conformational changes.[24,25,27−30] Other studies have probed various aspects of DHFR catalysis.[31−37] On the other hand, it has been argued that all these effects can be attributed to changes in reorganization energy.[26] We show that restriction of the conformational flexibility of the M20 loop at the transition state in the M42W/G121V double mutant is responsible for the impaired catalytic activity by causing an increase in the entropic barrier.

Before we begin, it is necessary to make clear the meaning of the term dynamics used here because the language itself is not without controversy.[1] Roughly, interpretations of dynamics in enzyme catalysis may be grouped into three categories: (i) transmission coefficient in rate theory, (ii) coherent protein motions with a transition state, and (iii) allosteric conformational change. One may argue that there is a fourth category, that there is no dynamic effect in enzyme catalysis, but it does not provide insight into enzyme mechanism and shall not be discussed further. In the first category, some researchers argue that the free energy of activation is an equilibrium quantity, which can be computed using either molecular dynamics or Monte Carlo simulations, and thereby, any dynamic effects must be in the transmission coefficient in rate theory. However, the transmission coefficient and the free energy of activation are interrelated, both depending on the reaction coordinate, which can be chosen to yield a unity transmission coefficient.[1,38] Thus, in this framework, "dynamics" lose meaning, except in nonequilibrium processes that are not known to play a significant role in enzyme-catalyzed reactions.[39] For the second proposal, it has been pointed out that there is no theoretical or experimental evidence supporting the coherent transfer of energy from protein motions to the transition state.[40] In this work, we adopt the third definition, which is used by most enzymologists,[20,41] to understand the specific role of protein conformational changes induced by the chemical transformation. These conformational changes, which may involve small shifts in the interatomic distances discussed by Benkovic and Hammes-Schiffer[24,25,29] or open−closed conformational fluctuations of loops in or remote from the active site[6,12,16,17,28,42] or dynamic fluctuations even without changes in the mean backbone conformation,[43] are allosteric transitions accompanying the chemical step[10] and, thus, are thermally averaged over the fast, local atomic fluctuations that may be important to barrier crossing at the transition state.[1]

In section I, we first present computational results for activation parameters and temperature-dependent KIEs. In this section, we establish that the impaired catalytic function in the M42W/G121V double mutant is due to reduced protein flexibility at the transition state relative to that in the wild-type DHFR. This accounts for the finding that the increased free energy barrier results predominantly from a reduction in the entropy of activation, i.e., increased entropic barrier in the double mutant.[13,20] Then, in section II, we identify a mechanism and show that the altered protein flexibility is related to restriction in loop conformational motions, mainly in the M20 and αE−F loop regions. The protein "dynamic knockout" in the M42W/G121V mutant can be attributed to an increased level of steric congestion at the mutation sites, particularly in the M42W mutation, resulting in an extra hydrogen bond to stabilize the closed conformation of the M20 loop. In section III, we make concluding remarks, and section IV provides a summary of a novel path integral free energy simulation method for computing kinetic isotope effects in enzymes along with computational details.

I. REDUCED PROTEIN FLEXIBILITY AT THE TRANSITION STATE IS RESPONSIBLE FOR IMPAIRED CATALYTIC EFFECTS IN THE M42W/G121V DOUBLE MUTANT

The change in reaction rate due to amino acid mutations, particularly those remote from the active site, is often smaller than the enormous rate enhancement caused by the enzyme relative to the uncatalyzed process in water,[44] but an understanding of the precise role of the altered protein structure in catalysis can be much more informative than the rate change itself. Thus, comparative studies of the wild-type enzyme and its mutants can be very useful in helping to identify a connection or absence of protein conformational dynamics with the catalyzed chemical step.[24−26,28] The main challenge is to evaluate accurately the small free energy changes induced by distal mutations to allow for analyses of structural and dynamic effects. This requires an accurate description of the potential energy surface for the chemical reaction,[45,46] and an extensive sampling to yield the potential of mean force as well as nuclear quantum effects (NQEs).[38,47] In the next section, we present detailed analyses of the dynamic trajectories, pointing to a role of reduced dynamic flexibility at the transition state in the M42W/G121V mutant relative to wild-type DHFR, and the restriction of a closed−open conformational transition of the M20 loop is responsible for the reduced dynamic fluctuation and increased entropy barrier in the chemical step.

A. Differences in the Catalytic Effect. The starting point in the computational study of enzyme catalysis is to determine the free energy of activation of the chemical step, and the relatively small changes in barrier height caused by mutations.[39,46] This requires an accurate potential energy surface to describe the chemical transformation, incorporating explicitly polarization effects in response to the dynamic fluctuations of the protein environment. We have developed a combined quantum mechanics/molecular mechanics (QM/MM) approach, in which the electronic structure of the hydride transfer is explicitly modeled by electronic structure theory.[39,45,48−50] In this case, the semiempirical AM1 Hamiltonian is used, along with a simple valence bond correction term specifically designed for the DHFR system,[30] and it has been used in a number of subsequent studies of DHFR.[39,49,51,52] We note that recently Major and co-workers reported a new parametrized AM1 model for DHFR hydride transfer.[34−36]

Using the same QM/MM methodology as in our earlier studies,[39,49,51,52] we obtained the potentials of mean force for the transfer of hydride from NADPH to DHF catalyzed by wild-type DHFR (wt-DHFR) and the M42W/G121V DHFR (dm-DHFR) at 5, 25, and 45 °C (Figure 2). In both cases, the free energy of activation, $\Delta G^{\ddagger}$, increases with temperature. At 25 °C, the computed $\Delta G^{\ddagger}$ for the hydride transfer is 16.4 kcal/mol for wt-DHFR, which may be compared with the experimental value of 16.7 kcal/mol determined at pH 9, under which the hydride transfer step is rate-limiting.[20] The activation free energy is increased by 1.2 kcal/mol in the M42W/G121V mutant, which is smaller than the corresponding experimental value (2.3 kcal/mol). Importantly, the experimental trends due to mutation are correctly reproduced. Inclusion of NQEs (see below) reduces the computed barrier by ∼3 kcal/mol for both wt- and dm-DHFR at 25 °C,[30,52] and the trend is not changed. The estimated free energies of reaction, ΔG_{rxn}, are approximately −5 and −2 kcal/mol for wt- and

dx.doi.org/10.1021/bi301559q | Biochemistry 2013, 52, 2036−2049

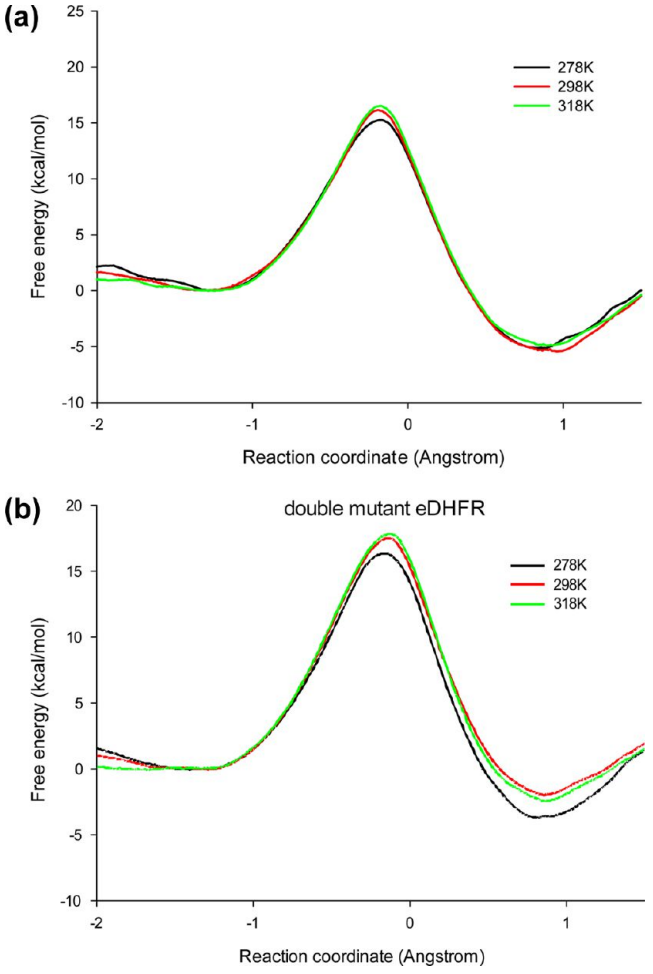

Figure 2. Computed classical mechanical potential of mean force for the hydride transfer in wild-type DHFR (a) and in the M42W/G121V double mutant (b) at 5, 25, and 45 °C. The reaction coordinate is defined as the difference in the distance of the transferring hydrogen (H4) from the donor carbon (C4N) of the cofactor and the acceptor carbon (C6) of the substrate.

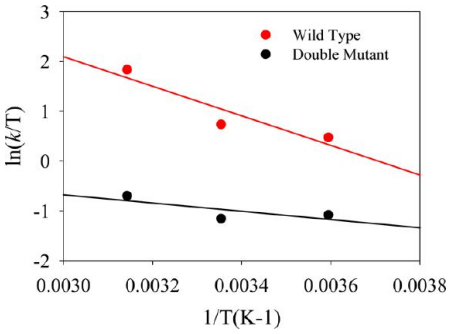

Figure 3. Eyring plots for hydride transfer in wt-DHFR (red) and the M42W/G121V mutant (black). Rate constants were determined using quantum transition state theory in which nuclear quantum effects were included in the estimated free energy barrier.

dm-DHFR, respectively, reflecting the fact that there is a small change in driving force for the hydride transfer caused by the M42W and G121V mutations. This is in accord with experimental data for the M42W/G121S mutant.[18,28] A similar effect of increasing the driving force and a correlation between free energy barrier and ΔG_{rxn} for a number of single- and double-mutant DHFR enzymes have been noted.[26]

B. Enthalpy and Entropy of Activation. The computed free energies of activation ($\Delta G^{\ddagger}$) for hydride transfer in wt- and dm-DHFR can be decomposed into enthalpy ($\Delta H^{\ddagger}$) and entropy ($\Delta S^{\ddagger}$) components using Eyring plot [$\ln(k/T)$ vs $1/T$] and transition state theory (Figure 3).[20,26,53] The slope ($-\Delta H^{\ddagger}/R$) yields the enthalpy of activation, and the intercept [$\ln(k_B/h) + \Delta S^{\ddagger}/R$] is converted to entropic contributions. This perhaps provides the most reliable estimate of the entropy of activation for an enzymatic reaction because direct computation of entropies at the reactant state and transition state would have much larger uncertainties than the entropy change itself,[54] whereas free energy simulations converge much more rapidly. The activation parameters provide important insights into the thermodynamic stabilization of the transition state (via $\Delta H^{\ddagger}$), and the contributions from dynamic fluctuations of the protein environment and the substrate that are transformed from the Michaelis complex to the transition state (through $\Delta S^{\ddagger}$).

The Eyring plots of the rate constants determined using the computed free energies of activation with the inclusion of NQEs are shown in Figure 3 for wt-DHFR and dm-DHFR, and the activation parameters are listed in Table 1. The corresponding experimental results at pH 9 are also listed for comparison. The results in Table 1 and Figure 3 are in agreement with the experimental data,[20] from which several conclusions can be drawn immediately. First, not surprisingly, there is a major compensating effect between enthalpy and entropy components in the activation of the hydride transfer, both in wt-DHFR and in the M42W/G121V double mutant. Of the two systems, a larger enthalpic barrier (suggesting weaker stabilizing interactions at the transition state) is accompanied by a smaller negative entropy of activation, i.e., greater dynamic flexibility because a reduction in the negative $\Delta S^{\ddagger}$ reflects enhanced flexibility at the transition state over the reactant state. Second, the enthalpy of activation is reduced by −4.3 kcal/mol in the double mutant relative to that of the wt-DHFR from computation, which may be compared with the experimental value of −1.7 kcal/mol.[20] Thus, counterintuitively, the double mutant, in fact, has a greater enthalpic stabilization of the transition state (thus reducing $\Delta H^{\ddagger}$) than the wild-type enzyme. Third, the computed and experimental entropies of activation are negative for hydride transfer both in the wild-type enzyme and in the M42W/G121V double mutant. Significantly, the entropy reduction becomes even more pronounced at the transition state as a result of the double mutation. In particular, the computed change in the entropy of activation, $\Delta\Delta S^{\ddagger}$, is −18.2 eu (cal mol^{-1} K^{-1}), while the corresponding experimental value is −13.2 eu;[20] these translate to free energies of 5.4 and 3.9 kcal/mol at 25 °C, respectively. The implication of these results both from experiment and from computation is that there is net reduction in the level of disorder, or dynamic flexibility, in going from the Michaelis complex to the transition state in the hydride transfer, and that the reduction in dynamic flexibility is greater in the M42W/G121V double mutant than in the wild-type enzyme. A similar reduction in $\Delta\Delta S^{\ddagger}$ has been noted in the G121V single mutant[19] and the N23PP/S148A double mutant.[12,13]

The total entropy of activation for hydride transfer in DHFR has several components (see discussions in refs 55 and 56), including the change in entropy of the intrinsic reaction coordinate of the substrate and cofactor ($\Delta S^{\ddagger}_{CS}$),the change in protein ($\Delta S^{\ddagger}_{Prot}$) and solvent ($\Delta S^{\ddagger}_{solv}$) fluctuations, and the change in translational and rotational entropy ($\Delta S^{\ddagger}_{tr}$) of the enzyme

dx.doi.org/10.1021/bi301559q | Biochemistry 2013, 52, 2036−2049

Table 1. Computed (including nuclear quantum effects) and Experimental Activation Parameters at 25 °C for Hydride Transfer in Wild-Type (wt) Dihydrofolate Reductase and the M42W/G121V Double Mutant (dm)

	computation			experiment		
	wt	dm	difference	wt	dm	difference
$\Delta H^{\ddagger}$ (kcal/mol)	5.9	1.6	−4.3	5.0 ± 0.6	3.3 ± 0.18	−1.7
$\Delta S^{\ddagger}$ (cal K^{-1} mol^{-1})	−25.4	−43.6	−18.2	−39.6 ± 1.0	−52.8 ± 1.3	−13.2
$\Delta G^{\ddagger}$ (kcal/mol)	13.5	14.7	1.2	16.7 ± 0.8	19.0 ± 0.4	2.3

complex as the substrate is transformed from the reactant to the transition state:

$$\Delta S^{\ddagger} = \Delta S^{\ddagger}_{CS} + \Delta S^{\ddagger}_{Prot} + \Delta S^{\ddagger}_{solv} + \Delta S^{\ddagger}_{tr} \quad (1)$$

The effect of single- and double-amino acid mutations on the overall translational and rotational entropy of the enzyme complex as well as on the surrounding solvent is expected to be negligible.[55,56] Consequently, the net change in $\Delta S^{\ddagger}$ due to amino acid mutation has two major contributions:

$$\Delta\Delta S^{\ddagger}_{mut} = \Delta S^{\ddagger}_{dm} - \Delta S^{\ddagger}_{wt} \approx \Delta\Delta S^{\ddagger}_{CS} + \Delta\Delta S^{\ddagger}_{Prot} \quad (2)$$

where $\Delta S^{\ddagger}_{wt}$ and $\Delta S^{\ddagger}_{dm}$ are the (total) entropy of activation for wild-type DHFR and the M42W/G121V double mutant, respectively, and $\Delta\Delta S^{\ddagger}_{CS}$ and $\Delta\Delta S^{\ddagger}_{Prot}$ are variations of the intrinsic reactant and the protein environment, respectively.

Because the transfer of hydride from NADPH to DHF brings two relatively large ligands together in covalent contact at the transition state, the first term in eq 1 ($\Delta S^{\ddagger}_{CS}$) is negative because of the loss of translational motions and the asymmetric mode associated with the reaction coordinate; they are closely related to the hydride acceptor and donor length (ADL). For the hydride transfer in wt-DHFR and the M42W/G121V double mutant, we found that the average ADLs are 3.50 and 3.46 Å at the Michaelis complex, respectively, and they are changed to 2.71 and 2.70 Å, respectively, at the transition state. As far as the acceptor−donor distance is concerned, there is no real difference in preorganizing the substrate and cofactor in the active site and in reaching the transition state as a result of the M42W/G121V double mutation, indicating that the net change in $\Delta\Delta S^{\ddagger}_{CS}$ is close to zero. Consequently, the large reduction in activation entropy estimated from molecular dynamics QM/MM simulations and determined experimentally (Table 1) may be attributed entirely to reduced protein flexibility at the transition state in the double mutant. Other studies have found widespread changes in the overall flexibility and coupled motions in mutant DHFR enzymes.[24,25,28]

$$\Delta\Delta S^{\ddagger}_{mut} \approx \Delta\Delta S^{\ddagger}_{Prot} \quad (3)$$

For comparison, an early study showed that the ADL is ∼3.45 Å at the Michaelis complex in wt-DHFR,[26] nearly the same as the present result. However, it was found that this distance was stretched by a half-angstrom to ∼4 Å in the M42W/G121V double mutant, and the distorted substrate−cofactor conformation in the Michaelis complex was found to increase the work term and thus the activation barrier by 1.8 kcal/mol relative to that of wt-DHFR.[26] An increased donor−acceptor distance was also proposed by Kohen and co-workers for the M42W/G121V double mutant.[20] We do not observe this elongated ADL in the double mutant. If anything, there seems to be a slight compression both in the Michaelis complex and in the transition state because both mutations introduce steric congestion propagated to the active site,[21,22] especially in the M42W mutation site[28] (see below).

Analyses in the next section demonstrate that the reduced dynamic flexibility at the transition state of the hydride transfer in the M42W/G121V double mutant relative to wt-DHFR is directly connected to the altered M20 loop motions in the active site.

C. Temperature Dependence of Kinetic Isotope Effects.

The altered protein motions due to amino acid mutations in the M42W/G121V enzyme are reflected in the observed KIEs. Wild-type *E. coli* DHFR exhibits a, now, general feature of temperature-independent KIEs for the hydride transfer step.[57] Intriguingly, the KIEs for the hydride transfer in M42W/G121V DHFR become steeply temperature-dependent.[20] In fact, a large number of enzymes have been found to show the temperature independence of KIEs in their optimal operating temperature range, but the KIEs are changed to temperature-dependent outside this temperature range or as a result of mutations.[4,11] The change in the temperature dependence of KIEs provides a direct probe of variations in transition state structure and its coupling to the enzyme environment.[13] Several studies have proposed that the wild-type enzyme has evolved to optimize the average donor−acceptor distance for tunneling at the transition state sampled by the mass-independent thermal activation, giving rise to temperature-independent KIEs (provided that tunneling is the dominant contribution to the observed KIEs).[4,11,20,58,59] However, ADLs are altered in mutant enzymes. Consequently, thermally activated "gating fluctuations" are required for effective tunneling in mutant enzymes such as in the M42W/G121V double mutant, leading to the temperature dependence of KIEs.[20]

Conceptually, there are two major contributions to the overall NQEs, responsible for the observed KIEs: the change in quantum vibrational free energy, predominantly zero-point effects, and tunneling.[38,49,52,60] For reactions in which tunneling is dominant, such as the hydrogen atom transfer catalyzed by soybean lipoxygenase,[61] the tunneling mechanism described above is quite reasonable. For the hydride transfer catalyzed by DHFR in which the observed intrinsic primary KIEs are only ∼3 both in wt-DHFR and in the mutants,[13,20,57] it would be important for a mechanism to also account for the contribution and change from the vibrational free energy. Previously, our group performed microscopic simulations of the small temperature dependence of the KIEs for the hydride transfer in wt-DHFR; in our approach, the dynamic simulations always include ADL thermal fluctuations automatically.[52] Using ensemble-averaged transition state theory including semiclassical multidimensional tunneling (EA-VTST/MT),[60,62] we identified two general features responsible for the observed temperature independence (or small temperature dependence) of KIEs in wt-DHFR: (a) variation of the transition state position and (b) temperature dependence of the effective potential for tunneling. In particular, we found that the location of the transition state for the hydride transfer coordinate is slightly shifted from −0.205 Å at 5 °C to −0.165 Å at 45 °C (Figure 4).[52] As a result, the difference in vibrational free energy between H-transfer and D-transfer is also increased at higher temperatures, resulting in a nearly temperature invariant Boltzmann factor. In this sense, there are greater NQEs at higher temperatures.

dx.doi.org/10.1021/bi301559q | *Biochemistry* 2013, 52, 2036−2049

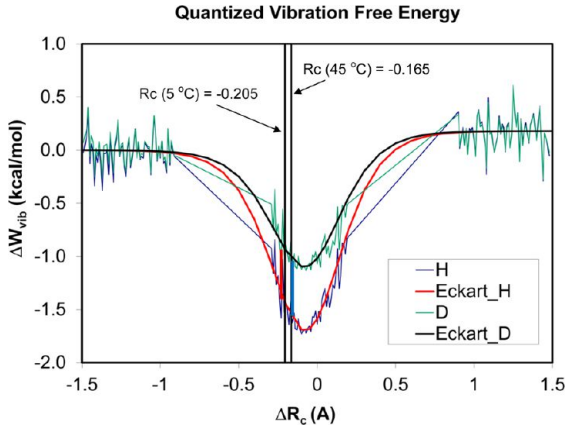

Figure 4. Computed average vibrational free energies for H-transfer (blue) and D-transfer (green) in wt-DHFR. The results are fit to an inverse Eckart function, and the locations of the transition state at 5 and 45 °C, determined after the vibrational free energies are included in the classical mechanical potential of mean force, are indicated by the vertical lines. The Boltzmann factor between H- and D-transfers gives the vibrational free energy contribution (dominantly zero-point effects) to the overall KIE (adapted from ref 52).

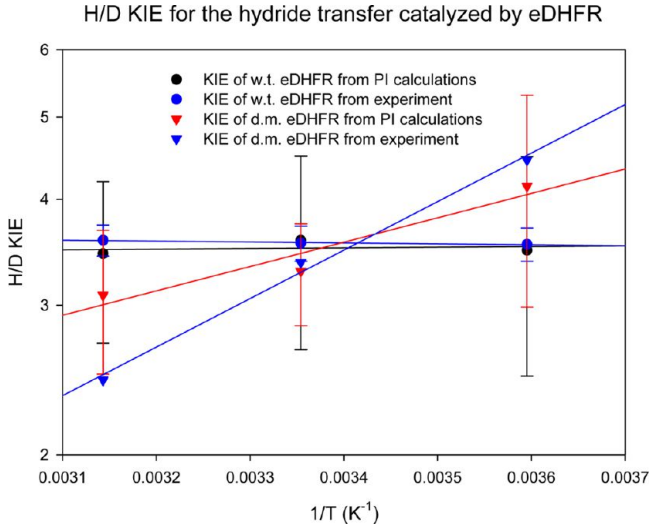

Figure 5. Comparison of the Arrhenius plots of experimental and computational intrinsic H−D kinetic isotope effects in wild-type and M42W/G121V mutant DHFR.

It is interesting to note that the difference in vibrational free energy is predominantly responsible for the computed H−D KIEs, with net values of 2.83 and 2.81 (without tunneling) at 5 and 45 °C, respectively; inclusion of tunneling increases the overall KIEs to 3.22 and 3.01, respectively, which is a small factor of only 14%.[52] Subsequently, other studies have also investigated the temperature dependence of KIEs in DHFR and its mutants.[63]

We further examined the temperature dependence of the KIEs for hydride transfer in both wt-DHFR and dm-DHFR using Feynman path integral simulations along with free energy perturbation on isotopic masses (which yields the necessary computational accuracy) and umbrella sampling over the reaction coordinate (which incorporates protein dynamic fluctuations); the method is called PI-FEP/UM.[64,65] Unlike the previous EA-VTST approach,[62] vibrational free energy and nuclear tunneling cannot be separated in path integral simulations, but the total NQEs as well as KIEs are obtained directly from statistical simulations. Nuclear quantum effects lower the free energy barrier from classical molecular dynamics simulations by ~2.8 ± 0.5 kcal/mol for wt-DHFR and dm-DHFR at 25 °C, in good accord with previous results (3.2 kcal/mol) computed using a completely different theoretical approach,[30,52] the EA-VTST/MT method. Our computed NQEs are somewhat greater than that estimated by other methods (~2 kcal/mol) in which only the hydride atom was quantized.[66,67] Arrhenius plots of the calculated and experimental H−D KIEs are shown in Figure 5. Good accord was obtained for wild-type DHFR in both the absolute value of KIEs and the temperature-independent behavior. The agreement for the M42W/G121V double mutant is also good, although the slope of the temperature dependence plot is smaller than that measured experimentally. Because the average ADLs are not different in the Michaelis complex and in the transition state between wt-DHFR and the M42W/G121V mutant, suggesting similar zero-point effects, we attribute the change in the temperature dependence of the KIEs in the double mutant to an altered potential energy surface for tunneling. The results shown in Figure 5 demonstrate that the absolute values and the trends in kinetic parameters as illustrated by the KIEs for hydride transfer, which directly report the structure and environment of the transition state, are correctly reproduced by the theoretical model.

II. REDUCED PROTEIN FLEXIBILITY AT THE TRANSITION STATE IN THE M42W/G121V MUTANT IS CAUSED BY CHANGES IN M20 LOOP CONFORMATIONAL DYNAMICS

The qualitative structure difference between wt-DHFR and the M42W/G121V double mutant in catalysis is immediately identified via inspection of the molecular dynamics trajectories along the hydride transfer pathway. In particular, at 25 °C, the M20 loop adopts a closed conformation in the Michaelis complex,[14] both in the wild type and in the double mutant (Figure 6, blue structures). However, at the transition state of hydride transfer, we found that the M20 loop undergoes a conformational transition in the wild-type enzyme, leading to a configuration resembling the open form (Figure 6a, brown) found in DHFR and the folate complex [Protein Data Bank (PDB) entry 1RD7]. Brooks and co-workers have noted that the closed conformation can be converted to the occluded state found in the product complex (PDB entry 1RX7) through the open conformation.[14,28] The M20 loop remained in the closed conformation throughout the hydride transfer pathway in the M42W/G121V double mutant (Figure 6b).

The M20 loop dynamics in the Michaelis complex and in the product complex have been studied by NMR relaxation experiments, and it has been implicated to play a critical role in DHFR catalysis.[6,12] To verify that the observed conformational transition in the transition state region was not due to artifacts of an incidental simulation during the umbrella sampling free energy calculations, we repeated these simulations twice at the transition state region of the wild-type enzyme, and carried out longer dynamics simulations in the regions of the reactant state (Michaelis complex) and the transition state, both for the wild-type and double mutant DHFR for 2.6 ns. In the Michaelis complex, the M20 loop fluctuates in the closed conformational substate in all cases for wt-DHFR and dm-DHFR. On the other hand, in both repeats of the umbrella sampling and the longer simulations, closed−open conformational transitions of the M20 loop took place in <100 ps in the wild-type enzyme, and it remained closed in the double mutant. We further compared the trajectories generated from simulations of wt-DHFR at 5 and 45 °C, which showed a greater extent of M20 loop opening at 45 °C after the transition state, whereas the M20 loop was closed

dx.doi.org/10.1021/bi301559q | *Biochemistry* 2013, 52, 2036−2049

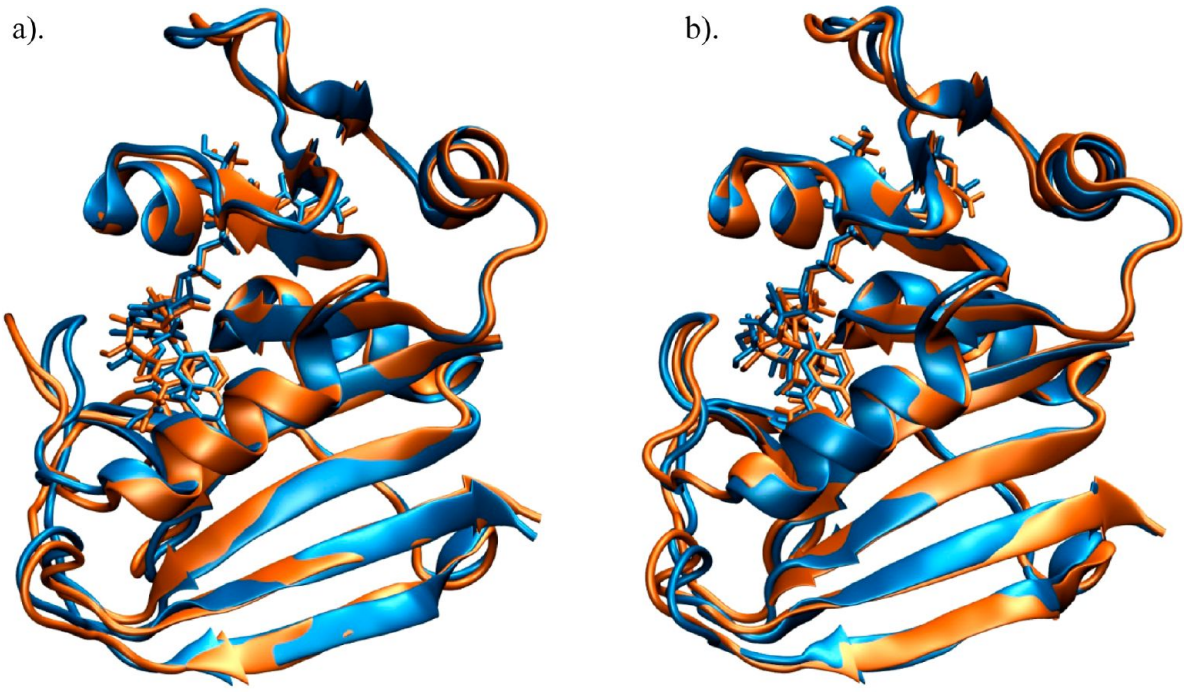

Figure 6. Comparison of snapshot structures in the reactant state (Michaelis complex, blue) and in the transition state (brown) for hydride transfer in wt-DHFR (a) and the M42W/G121V double mutant (b).

along the hydride transfer pathway at 5 °C. On the other hand, the M20 loop conformation was closed throughout the simulations of the M42W/G121V double mutant at all three temperatures. These findings suggest that, qualitatively, at physiologically relevant temperatures, the M20 loop undergoes conformational transitions as the hydride transfer reaction coordinate reaches the transition state region in wt-DHFR; however, this conformational change is quenched in the M42W/G121V double mutant. The differential M20 loop dynamics is likely to be responsible for the difference in the temperature dependence of KIEs.

The coupling between M42 and G121 sites has been extensively studied, and its impact on loop dynamic fluctuations of DHFR has been well established through mutation, kinetic, and NMR experiments.[18,19,21,22,68−70] Mauldin et al. showed that the M20 loop adopts the closed conformation in the ternary complex with NADPH and methotrexate in the M42W and G121V mutants.[21,22] While the G121V mutantion results in a large response on the M42 dynamic fluctuations from NMR relaxation experiments,[21] the M42W mutation showed that the M42 site serves has a hub connecting the dynamic fluctuations throughout the protein.[22] The M20 conformational fluctuations in wt-DHFR and single and double mutants at M42 and G121 as well as their coupled motions in the Michaelis complex have been examined by Brooks and co-workers.[27,28,71,72] It was found that there are several pathways between the closed and open conformations, with different mutants favoring some particular routes. For example, both the G121S mutant and wt-DHFR went through a similar intermediate state to reach an openlike conformation, although they did not move all the way to the open conformation as in the crystal structure of PDB entry 1XD7.[28]

To provide a more quantitative assessment of the conformational fluctuations along the hydride transfer pathway, we computed the mean square fluctuations (MSF) of the backbone C_α atoms for the reactant state (RS) and transition state (TS) for wt-DHFR and dm-DHFR, making use of the 2.6 ns trajectories.

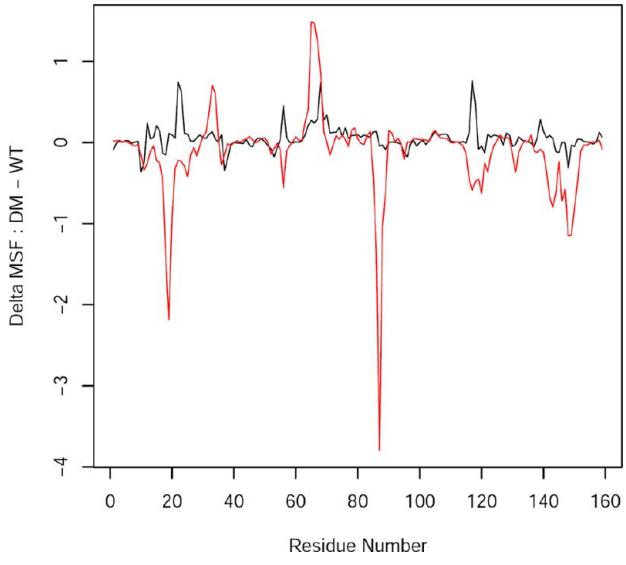

Figure 7. Difference in mean square fluctuations (MSF) of backbone C_α atoms between wild-type DHFR and the M42W/G121V double mutant, MSF[dm] − MSF[wt], in the Michaelis complex reactant state (black) and transition state (red). Negative values indicate regions with greater structural fluctuations in the wt enzyme, whereas positive regions reflect enhanced fluctuations in the dm enzyme.

The changes in MSF from wt-DHFR to dm-DHFR at the RS (black) and the TS (red) are displayed in Figure 7. In these plots, negative values correspond to reduced fluctuations in the double mutant (i.e., greater fluctuations in the wild-type enzyme), while positive values indicate enhanced dynamic fluctuations caused by the double-amino acid mutations. Overall, the dynamic fluctuations are very similar in the Michaelis complex between wt- and dm-DHFR, although several regions exhibit somewhat increased fluctuations in the double mutant. However, significant differences between wt-DHFR and the M42W/G121V double mutant

dx.doi.org/10.1021/bi301559q | *Biochemistry* 2013, 52, 2036−2049

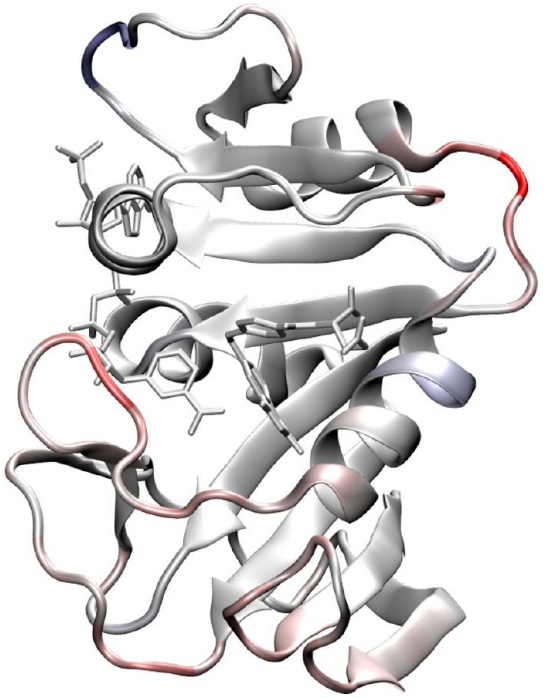

Figure 8. Illustration of regional variations between wild-type DHFR and the M42W/G121V double mutant in going from the reactant state (Michaelis complex) to the transition state. This corresponds to the difference between the two MSFs shown in Figure 7. Regions showing reduced fluctuations to reach the transition state in the double mutant relative to that in the wild-type enzyme are colored red, while enhanced fluctuations are colored blue (almost nonexistent except the C−D loop region on the top).

are found in several key regions in the DHFR structure at the transition state region of the hydride transfer (Figures 7 and 8). In particular, the M20 loop (around amino acid 18) and the αE−F loop (at amino acid 87) show significantly reduced fluctuations in the double mutant versus wt-DHFR, and dampened fluctuations are also found in the F−G loop (around residue 119) and the G−H loop in the region of residues 140−150. There are two regions in the double mutant that show increased motions relative to the wild-type enzyme at the transition state, although the magnitude is much smaller than reduced motions; they are located at the end of the αB helix and in the C−D loop. Figures 7 and 8 paint a picture that while the M42W/G121V double mutation has relatively small effects on the dynamic fluctuations in the Michaelis complex, it causes major changes in dynamic fluctuations at the transition state in key regions for hydride transfer, predominantly a reduction in nature relative to wt-DHFR. We suggest that the restricted M20 and E−F loop conformation dynamics at the transition state in M42W/G121V DHFR is responsible for the computed decrease in activation entropy. (Note that we have not addressed the difference in loop flexibility of the apo enzymes and its influence on substrate and cofactor binding.)

Recently, Bhabha designed a different double mutant, N23PP/S138A, aimed to restrict the M20 loop conformational motions.[12] However, the N23PP/S138A mutant has a relatively minor effect on rate reduction,[12] and it was subsequently found that the temperature dependence of KIEs was not affected compared with that of the wild-type enzyme.[13] As a result, it was suggested that that double mutation did not achieve the original goal of restricting M20 loop dynamics.[13] Nevertheless, the entropy of activation is reduced by 5.3 eu in the N23PP/S138A enzyme,[13] indicating that protein fluctuations are reduced at the transition state. Here, we found that the impaired catalytic function in the M42W/G121V mutant is also a result of the M20 loop "dynamic knockout".

The altered loop conformational dynamics between the wild-type and M42W/G121V double mutant DHFR enzymes can be characterized by low-frequency quasi-harmonic motions. To highlight this important property and the motions that are suppressed at the TS of the hydride transfer in the double mutant relative to that in wt-DHFR, we conducted principal component analyses (PCA)[54] by diagonalizing the covariant matrices of the atomic displacements for wt-DHFR and dm-DHFR in the RS and TS. The PCA results show the directionality and frequency of protein dynamic motions, in which the lowest-frequency modes are typically correlated with protein conformational changes and have been used to interpret conformational variations observed experimentally.[7,73] The dynamic motions of the lowest-frequency mode (stretched by variations up to 2σ from the mean) for the four states considered are illustrated in Figure 9. The fluctuations resulting from the lowest-frequency mode contribute ∼25% of the total dynamic motions of the enzyme in each case, whereas the contributions from the next mode are reduced to ∼6%. Thus, Figure 9 provides key features of the dynamic motions in each system. Of the four different simulations (wt-RS, wt-TS, dm-RS, and dm-TS) in Figure 9, we immediately notice that the dominant motions of the wt-TS state are characterized by the closed−open conformational transition of the M20 loop. This is different from the three other states in which the M20 loop remains in the closed form. The most significant motions at the TS in the M42W/G121V double mutant occur in the C−D loop and αE−F loop regions. The difference in quasi-harmonic motions from a single, lowest-frequency mode is in remarkably good accord with the overall MSF in Figure 8, except in the αE−F loop region at the TS, where contributions from other modes are also important in the wild-type enzyme. Importantly, the PCA analyses provide a dynamic mechanism (not promoting modes or motions) connecting quasi-harmonic motions of the protein, particularly in the closed−open conformational transition of the M20 loop, with average conformational changes along the hydride transfer coordinate in wt-DHFR.

The structural origin responsible for the altered dynamic fluctuations of the enzyme at the transition state due to the M42W/G121V double mutation is illustrated in Figure 10, which depicts key hydrogen bonding interactions that maintain M20 loop closure. In the reactant state (Michaelis complex) of the wild-type enzyme, Q18 forms two hydrogen bonds, one donating the backbone amide hydrogen to the 3′-hydroxyl oxygen and another accepting a bond from the side chain of H45 by the carbonyl group of the Q18 side chain. Apparently, these interactions are not sufficient to maintain the M20 loop in the closed conformational substate, perhaps because of the altered electron density of the substrate and cofactor at the transition state, breaking away to adopt a more open form. In the double mutant, the M42W mutation imposes steric congestion due to the large size of Trp in comparison with Met, which pushes the αC helix toward the M20 loop. This shifts the side chain of S49 from donating a hydrogen bond to the backbone carbonyl group of H45 to forming a hydrogen bond to the carbonyl oxygen of the Q18 side chain. Thus, there is an additional hydrogen bond interacting with the M20 loop, sufficient to keep its conformation in the closed form throughout the hydride transfer process. Note that W42 is sandwiched between

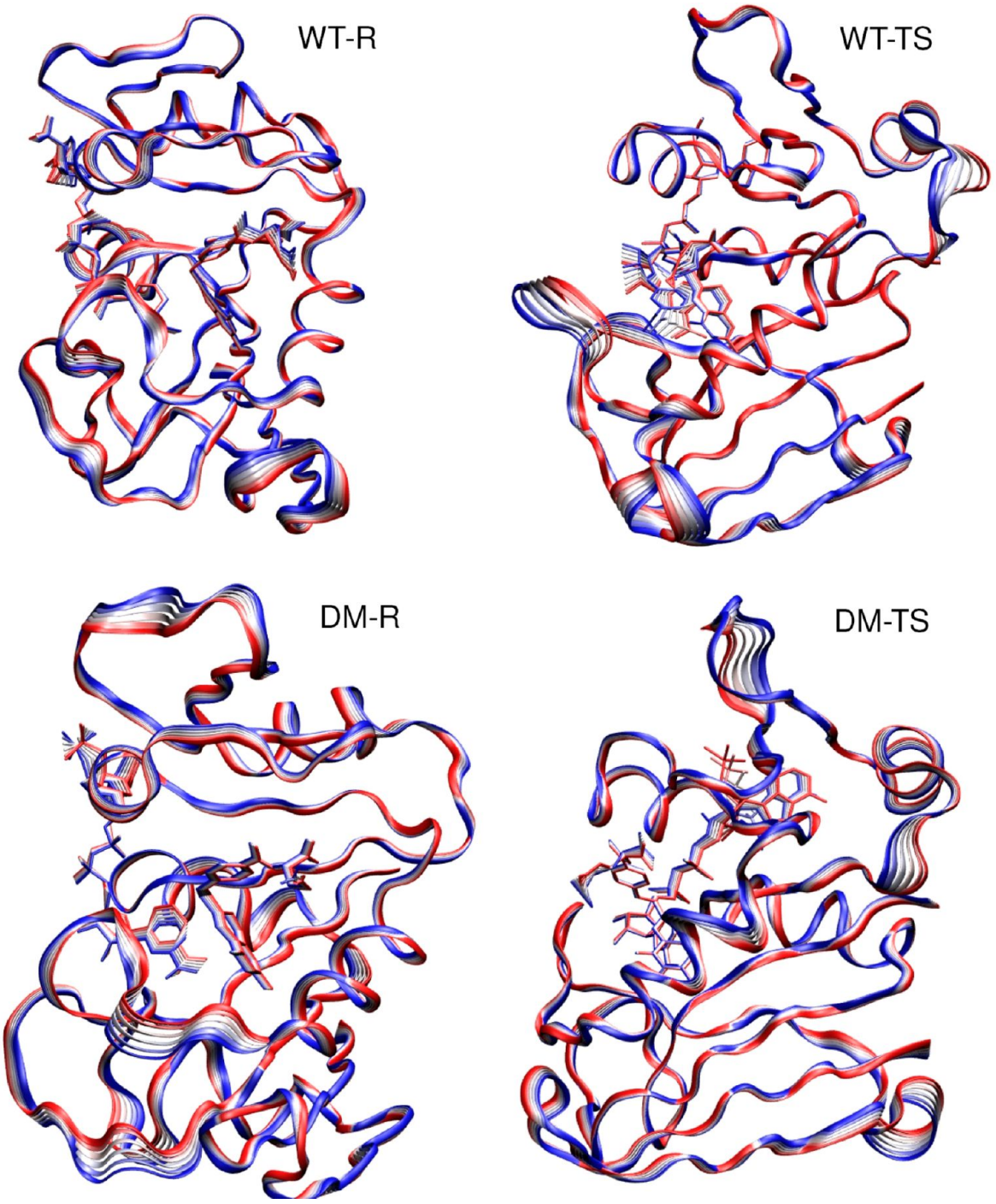

Figure 9. Illustration of the dynamic motions of the lowest-frequency quasi-harmonic mode for the wild type (WT) and M42W/G121V double mutant (DM) in the reactant state (RS) and transition state (TS). A sequence of six structures stretched up to 2σ from the mean are superimposed.

helices αC and αE, which in turn quench dynamic fluctuations of the αE−F loop.

III. CONCLUDING REMARKS

Combined QM/MM molecular dynamics simulations of hydride transfer in wt-DHFR and the M42W/G121V double mutant were conducted at three different temperatures (5, 25, and 45 °C). The computed changes in activation parameters due to amino acid mutations are in reasonable accord with experiment. The dominant factor responsible for the impaired catalytic function in the mutant enzyme is the reduced dynamic flexibility at the transition state, giving rise to an increased free energy barrier. Although it is counterintuitive, the double mutation in fact enhances enthalpic stabilization of the transition state over the wild-type enzyme. It was found that the average acceptor−donor lengths for the hydride transfer are essentially the same in the Michaelis complex (~3.5 Å) and the transition state (2.7 Å) for wt-DHFR and the M42W/G121V double mutant, implying that the change in the intrinsic entropy of activation, $\Delta\Delta S^{\ddagger}_{CS}$, of the cofactor and substrate due to mutations is negligible. Consequently, the overall reduction in $\Delta S^{\ddagger}$ may be attributed to reduced protein flexibilities at the transition state in the double mutant relative to that of the wild-type enzyme.

dx.doi.org/10.1021/bi301559q | *Biochemistry* 2013, 52, 2036−2049

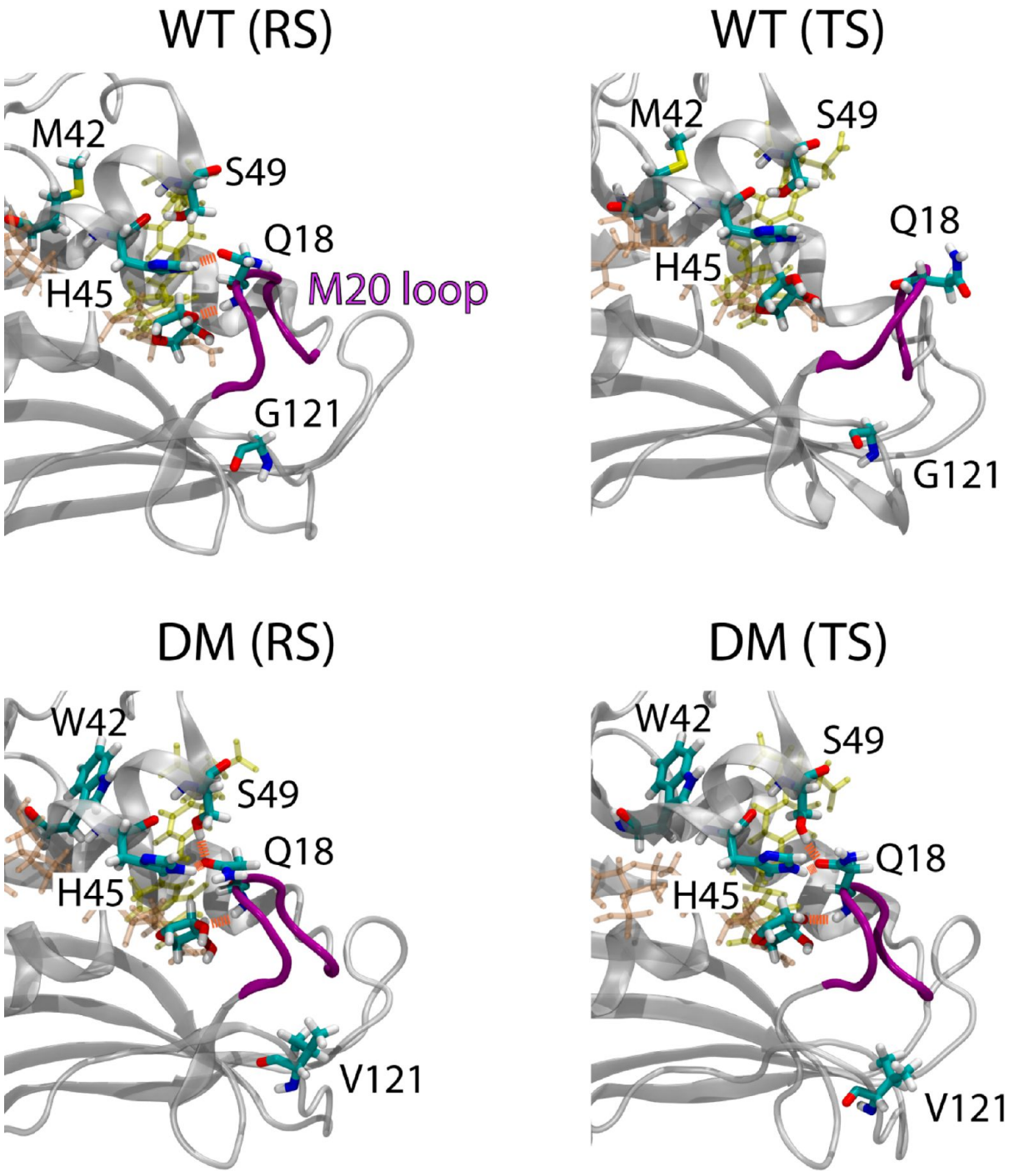

Figure 10. Structures highlighting hydrogen bonding interactions between Q18 of the M20 loop and the cofactor sugar and amino acids (H45 and S49) of helix αC. M42 in wt-DHFR and W42 in the double mutant are shown as stick models in the back of helix αC.

Structural and principal component analyses of the dynamic trajectories reveal that loop conformational fluctuations are severely dampened in the transition state region as a result of mutation, whereas there is increased flexibility in the Michaelis complex. Significantly, the altered protein fluctuations are found to be associated with the allosteric conformational transition of the M20 loop between the closed (Michaelis complex) and open forms accompanying the chemical transformation. In particular, we found that the M20 loop, which is known to be critical to DHFR catalysis, can sample the openlike conformations near the transition state of hydride transfer in wild-type DHFR. However, the M20 loop remains closed in the double mutant. We further identified that, because of the M42W/G121V double mutation, the hydrogen bond between S49 and the H45 carbonyl oxygen in helix αC is shifted to interact with the side chain of Q18 of the M20 loop. Thus, the extra hydrogen bonding interaction with the M20 loop in the M42W/G121V double mutant stabilizes the closed M20 conformation, resulting in a net reduction in protein allosteric conformational flexibility at the transition state. The computational results appear to mirror the model of a different double mutant, N23PP/S148A,[12] which was designed precisely to knock out the dynamic flexibility of the M20 loop. In that case, the entropy of activation was also reduced, implicating the reduced protein flexibility of the transition state relative to that of

dx.doi.org/10.1021/bi301559q | *Biochemistry* 2013, 52, 2036−2049

the wild-type enzyme; however, kinetic parameters, both in the rate and in the temperature dependence of KIEs, were not significantly affected.[13]

This finding that restricted allosteric conformational flexibility of the M20 loop is a main factor responsible for the increased entropic barrier (more negative entropy of activation) in the M42W/G121V double mutant is not inconsistent with the reorganization model.[13,20,26,63] It was pointed out that perturbations to the protein structure from distant mutations can propagate to the active site, resulting in elongated donor−acceptor distances[20] and increased reorganization energy relative to that in the wild-type enzyme.[26,63] This hypothesis focuses on the "distance" of the energy gap coordinate or preorganization of the substrate and cofactor in the enzyme environment. Implicitly, it emphasizes that the linear response force constant for protein reorganization is similar (but not required) in the wild-type enzyme and in the mutant enzyme. In addition, an elongated donor−acceptor distance would pay more reorganization energy, hence and increased free energy barrier (Scheme 1a). This is very reasonable indeed. The present model can be put in the same context (Scheme 1b), where the preorganization effects are similar in wild-type and mutant DHFR as far as the acceptor−donor distance for the hydride transfer is concerned. However, the force constants for the Marcus parabola are greater in the mutant enzyme than in wild-type DHFR, thanks to reduced flexibility in loop conformational dynamics. Thus, the reduced entropy of activation is reported by an increased slope in the Marcus-type diabatic states (Scheme 1). Both mechanisms are possible depending on the specific enzymes.

Scheme 1. Description of Extreme Models Using Protein Reorganization Energy[a]

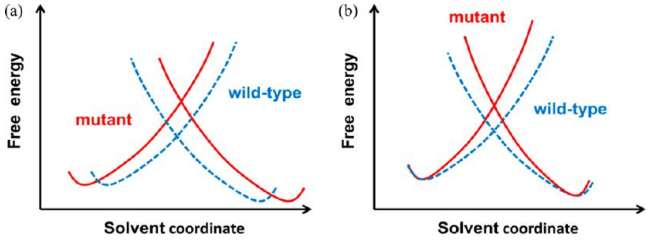

[a]In model a, the preorganization effect is disrupted because of distant mutations along with an increased donor−acceptor distance (not shown in the energy gap coordinate). This results in a greater reorganization energy, i.e., free energy barrier, to reach the transition state at the diabatic crossing point. In model b, the donor and acceptor species have the same distance and preorganization effect in the Michaelis complex in both the wild-type and double-mutant enzymes, but remote mutations affect protein conformational flexibility toward the transition state, which is reported by an increased force constant for the protein response in the diabatic picture.

The fact that the impaired catalytic activity by the M42W/G121V double mutation is due to the increased entropic barrier relative to that of the wild-type enzyme was known long ago;[18,20] however, its mechanistic implication has not been emphasized. Benkovic and co-workers pointed out that while the coupling between distal residues M42 and G121 and their roles in catalysis may be inferred from kinetic data, "the physical nature of the process is not known".[18] The study presented here favors a mechanism in which regional changes in the conformational heterogeneity of the enzyme, accompanying the chemical transformation from the Michaelis complex to the transition state, are important to catalysis, and the effects are expressed primarily in the entropy of activation, $\Delta S^{\ddagger}$. Consequently, increased dynamic fluctuations of the protein in the transition state over the Michaelis complex are entropically favored for the catalyzed reaction, although stabilization of the transition state can be a dominant factor to lower the free energy barrier in catalysis.

This mechanism may be considered as an extension of the "ensemble" view of protein allostery that has emerged in recent years.[10,43,74,75] In this picture, rather than an induced transition from a well-defined inactive state to an active configuration as in the classical allosteric models,[76,77] the binding at the allosteric site shifts the population of a conformational ensemble toward the active state. In fact, this shift may not necessarily require a change in the mean backbone conformation of the protein.[43] Here, the allosteric effector is the chemical transformation itself. The connection between protein dynamics and enzyme catalysis is not in the precise time-dependent transition and trajectory between the inactive and active states, e.g., from the Michaelis complex to the transition state. Instead, the conformational ensemble of the enzyme−substrate complex encompasses all these substates (the existence of such conformational ensembles has been demonstrated for the entire DHFR catalytic cycle),[6,28] and it is the population of the protein corresponding to the Michaelis complex that is shifted toward a population in the transition state as a result of the thermal activation of the chemical reaction. One may prefer that this be purely an equilibrium, thermodynamic phenomenon, not a dynamic effect. However, there are differences in protein dynamic fluctuation and in conformational sampling between the Michaelis complex and the transition state in an enzymatic process, and an understanding of the contributions from dynamic fluctuations to catalysis and their changes as a result of amino acid mutation is useful. In DHFR, the wild-type enzyme is capable of sampling a greater range of conformational space, especially involving the M20 loop motions, whereas in the M42W/G121V double mutant, the conformational heterogeneity is restricted at the transition state in several loop regions.

IV. METHODS

We provide a brief summary of the integrated path integral and free energy simulation method used to determine kinetic isotope effects for enzymatic reactions,[65] and a summary of the key computational details. The key novel contribution is to conduct free energy perturbation of different isotopic masses in a single dynamics simulation.[65] Consequently, both primary and secondary, as well as heavy atom, KIEs can be accurately determined from statistical simulations.[78,79]

A. Quantum Transition State Theory and Path Integral Simulations of KIEs. The theoretical framework in our discussion is path integral quantum transition state theory (QTST),[80−82] which is derived by writing the rate expression in a manner analogous to classical transition state theory.

$$k_{\mathrm{QTST}} = \frac{1}{2}\left\langle |\dot{z}| \right\rangle_{z^{\ddagger}} e^{-\beta w(z^{\ddagger})} \Big/ \int_{-\infty}^{z^{\ddagger}} dz\, e^{-\beta w(z)} \tag{4}$$

where $w(z)$ is the potential of mean force (PMF) as a function of the centroid reaction coordinate $z[\bar{\mathbf{r}}]$, $z^{\ddagger}$ is the value of $z[\bar{\mathbf{r}}]$ at the maximum of the PMF, and $\langle|\dot{z}|\rangle_{z^{\ddagger}} = (2k_{\mathrm{B}}T/\pi M_{\mathrm{eff}})^{1/2}$ is a dynamical frequency factor approximated by the velocity for a free particle of effective mass M_{eff} along the reaction coordinate direction. The centroid coordinate of particle n in path integral simulation is defined by $\bar{\mathbf{r}}^{(n)} = \sum_{i=1}^{P} \mathbf{r}_i^{(n)}/P$, where P is the number of discrete particles with the corresponding coordinates $\{\mathbf{r}_i^{(n)}\}$.

dx.doi.org/10.1021/bi301559q | Biochemistry 2013, 52, 2036−2049

The exact rate constant is obtained by multiplying the QTST rate constant by a correction factor or transmission coefficient γ_q:[81]

$$k = \gamma_q k_{QTST} \tag{5}$$

Equations 4 and 5 have forms identical to that of the classical rate constant, but unlike transition state theory, there is no variational upper bound in the QTST rate constant because the quantum transmission coefficient γ_q may be either greater or less than 1. There is no practical procedure for computing the quantum transmission coefficient γ_q. For a model reaction with a parabolic barrier along the reaction coordinate coupled to a bath of harmonic oscillators, the quantum transmission coefficient is the Grote−Hynes (GH) classical transmission coefficient κ_{GH}.[83] Often, the classical γ_q is used to approximate the quantum transmission coefficient; however, there is no correspondence between classical and quantum dynamic trajectories, and the effects of tunneling may greatly affect reaction dynamics near the top of the barrier.

As in classical transition state theory, the PMF including nuclear quantum effects, $w(z)$, can be computed from the equilibrium averages of a double-average procedure:[84,85]

$$e^{-\beta w(\bar{z})} = e^{-\beta w_{cm}(z)} \left\langle \delta(z = \bar{z}) \left\langle e^{-\beta \Delta \bar{U}(\bar{z}[\mathbf{r}],\mathbf{S})} \right\rangle_{FP,\bar{z}} \right\rangle_U \tag{6}$$

where $w(\bar{z})$ and $\bar{z}_{cm}(z)$ are the centroid quantum mechanical and the classical mechanical (CM) PMF, respectively, $\Delta\bar{U}(\bar{\mathbf{r}},\mathbf{S})$ is the difference in potential energy between the QM and CM systems,[84,86,87] the ensemble average $\langle\cdots\rangle_U$ is obtained from classical molecular dynamics simulations using the potential $\bar{U}(\bar{\mathbf{r}},\mathbf{S})$, and the inner average is carried out through path integral free-particle sampling over configurations generated from the classical trajectories. The double-averaging approach was used by Sprik et al. in Monte Carlos simulations, called the hybrid classical and path integral,[86] and used in enzyme calculations by Hwang and Warshel, called the quantized classical path,[87] and by our group in coupled free energy perturbation and umbrella sampling (PI-FEP/UM) simulations.[65]

The centroid path integral method allows us to conveniently determine KIEs by directly computing the ratio of the quantum partition functions for two different isotopes through free energy perturbation (FEP) theory.

$$KIE = \frac{k^L}{k^H} = \left[\frac{Q_{qm}^{L}(\bar{z}_L^{\ddagger})}{Q_{qm}^{H}(\bar{z}_H^{\ddagger})}\right]\left[\frac{Q_{qm}^{H}(\bar{z}_H^{R})}{Q_{qm}^{L}(\bar{z}_L^{R})}\right] e^{-\beta[F_L^R(\bar{z}_L^R) - F_H^R(\bar{z}_H^R)]} \tag{7}$$

with

$$\frac{Q_{qm}^{H}(\bar{z})}{Q_{qm}^{L}(\bar{z})} = \frac{\left\langle \delta(z-\bar{z}) \left\langle e^{-\beta/P \sum_i \Delta U_i^{L\to H}} e^{-\beta \Delta \bar{U}_L} \right\rangle_{FP,L} \right\rangle_U}{\left\langle \delta(z-\bar{z}) e^{-\beta[F_L(\bar{z},\mathbf{S}) - F_{FP}^{\circ}]} \right\rangle_U} \tag{8}$$

where a subscript L specifies that the ensemble averages are done using the light isotope, F_{FP}° is the free energy of the free particle reference state for the quantized particles,[84] and $\Delta U_i^{L\to H} = U(\mathbf{r}_{i,H}) - U(\mathbf{r}_{i,L})$ represents the difference in "classical" potential energy at heavy and light bead positions $\mathbf{r}_{i,H}$ and $\mathbf{r}_{i,L}$, respectively.

In essence, only one simulation of a given isotopic reaction, e.g., the light isotope, is performed, while the ratio of the partition function, i.e., the KIE, to a different isotopic reaction, is obtained through FEP by perturbing the mass from the light isotope to the heavy isotope.[65] A bisection sampling technique was extended to centroid path integral simulations to obtain converged results.[64] This is in contrast to other approaches that have been reported in the literature employing centroid path integral simulations,[87−89] in which two separate simulations are performed. The use of "mass" perturbation in a free-particle bisection sampling scheme results in a major improvement in computational accuracy for KIE calculations such that secondary kinetic isotope effects and heavy atom isotope effects can be reliably obtained.[65,78,90] To the best of our knowledge, the coupled path integral free energy perturbation and umbrella sampling (PI-FEP/UM) method is the only practical approach to yield computed secondary KIEs sufficiently accurate to be compared with experiments.[79]

B. Combined QM/MM Potential Energy Surface. The accuracy of the potential energy function used to conduct molecular dynamics simulations directly affects the reliability of the computed $w(\bar{z})$. We employ combined QM/MM methods,[46,91] in which the hydride transfer catalyzed by DHFR is modeled by a reaction specific parametrized AM1 model[92] with a simple valence bond correction described in ref 30 and the rest of the system is represented by the CHARMM22 force field.[45,50] The QM/MM potential is given by[91]

$$U_{tot} = \langle \Psi(S)|H_{qm}^{\circ}(S) + H_{qm/mm}(S)|\Psi(S)\rangle + U_{mm} \tag{9}$$

where $H_{qm}^{\circ}(S)$ is the Hamiltonian of the QM subsystem, U_{mm} is the classical (MM) potential energy for the MM region, and $H_{qm/mm}(S)$ is the interaction Hamiltonian between the two regions. The wild-type DHFR system[14] was partitioned into 69 quantum mechanical atoms (N_{QM}) and 21399 classical mechanical atoms (N_{MM}). The QM system (Scheme 2) includes 39 atoms of the DHF substrate

Scheme 2. Representation of Atoms Treated Explicitly by Electronic Structure Theory and by Molecular Mechanics for the NADPH Cofactor (top) and 7,8-Dihydrofolate Substrate (bottom)[a]

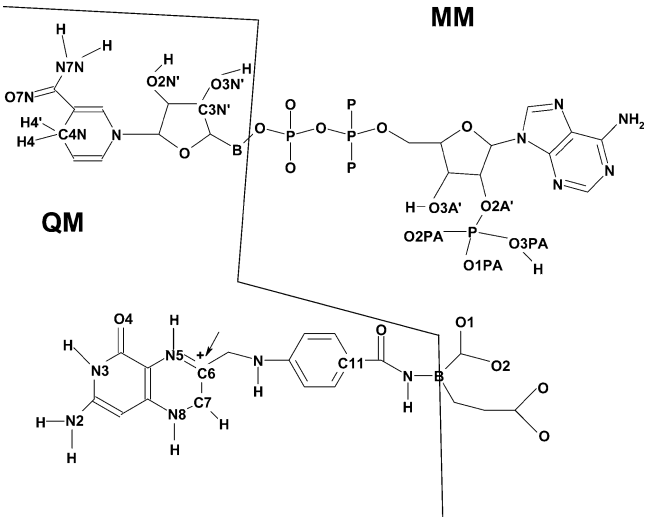

[a]The symbol B indicates a boundary atom that is treated both as a QM and as an MM atom in the generalized hybrid orbital (GHO) method. Adapted from ref 30 with permission from the American Chemical Society.

(the pteridine ring, the pABA moiety, and the -NH-C_α group of the glutamate moiety) and 30 atoms of the NADPH cofactor (the dihydronicotinamide and ribose rings). This QM subsystem contains two boundary atoms: the C_α atom at the glutamate moiety

dx.doi.org/10.1021/bi301559q | Biochemistry 2013, 52, 2036−2049

and the C5 ribose atom, which are treated partly by MM and partly with the generalized hybrid orbital (GHO) method.

C. Computational Details. The starting structures for the simulations of wild-type eDHFR at the three temperatures were taken from the simulations conducted previously.[30,52] These structures were re-equilibrated at their respective temperatures with a constant pressure of 1 atm for 100 ps. The M42W/G121V double-mutant structures were built by performing in silico mutation on the wild-type enzyme structures and were subject to 200 ps equilibration using the *NPT* ensemble. All equilibrations were conducted using the QM/MM potential detailed in ref 30.

The periodic boundary conditions are employed to solvate the system. A cubic water box is used to solvate the entire Michaelis complex, with dimensions of ∼60 Å × ∼60 Å × ∼60 Å. The simulation was performed corresponding to pH 7 by adjusting the protonation state of histidine residues, and all polar amino acid residue side chains are protonated and deprotonated accordingly. The resulting Michaelis complex bears 15 units of negative charge, and it is neutralized by randomly placing 15 sodium ions in the water box. A spherical cutoff distance of 12 Å was used for the nonbonded interactions, with a switch function in the region between 11 and 12 Å. The pressure (at 1 atm) and the temperature of the systems were controlled with the Nosé-Hoover extended system method. A total of 16 simulation windows were used to encompass the reaction coordinate from −2.0 to 1.5 Å, which is defined as the difference between the transferring hydride from the donor carbon on NADPH and the acceptor carbon of DHF. Each simulation window was subjected to further equilibration for at least 100 ps followed by 170−220 ps averaging. Thus, each potential of mean force was averaged over 4−5 ns simulations. The kinetic isotope effects were averaged over at least 24000 configurations at each temperature.

■ ASSOCIATED CONTENT

Supporting Information

One table of computed data, including free energies of activation at different temperatures. This material is available free of charge via the Internet at http://pubs.acs.org.

■ AUTHOR INFORMATION

Corresponding Author

*Telephone: (612) 625-0769. E-mail: gao@jialigao.org.

Present Address

[†]Department of Chemistry, Towson University, 8000 York Rd., Towson, MD 21252.

Funding

This work was supported by National Institutes of Health Grant GM46367.

Notes

The authors declare no competing financial interest.

■ ABBREVIATIONS

ADL, acceptor−donor length; DHF, 7,8-dihydrofolate; DHFR, dihydrofolate reductase; dm, double mutant; EA-VTST/MT, ensemble-averaged transition state theory with multidimensional tunneling; KIE, kinetic isotope effect; NADPH, nicotinamide adenine dinucleotide phosphate; NQE, nuclear quantum effect; PCA, principal component analysis; PI-FEP/UM, path integral free energy perturbation and umbrella sampling; PMF, potential of mean force; QM/MM, quantum mechanics/molecular mechanics; QTST, quantum transition state theory; RS, reactant state; TS, transition state; wt, wild-type.

■ REFERENCES

(1) Antoniou, D., and Schwartz, S. D. (2011) Protein Dynamics and Enzymatic Chemical Barrier Passage. *J. Phys. Chem. B 115*, 15147−15158.

(2) Boehr, D. D., Dyson, H. J., and Wright, P. E. (2006) An NMR perspective on enzyme dynamics. *Chem. Rev. 106*, 3055−3079.

(3) Hay, S., and Scrutton, N. S. (2012) Good vibrations in enzyme-catalysed reactions. *Nat. Chem. 4*, 161−168.

(4) Nagel, Z. D., and Klinman, J. P. (2009) A 21st century revisionist's view at a turning point in enzymology. *Nat. Chem. Biol. 5*, 543−550.

(5) Glowacki, D. R., Harvey, J. N., and Mulholland, A. J. (2012) Taking Ockham's razor to enzyme dynamics and catalysis. *Nat. Chem. 4*, 169−176.

(6) Boehr, D. D., McElheny, D., Dyson, H. J., and Wright, P. E. (2006) The dynamic energy landscape of dihydrofolate reductase catalysis. *Science 313*, 1638−1642.

(7) Henzler-Wildman, K. A., Thai, V., Lei, M., Ott, M., Wolf-Watz, M., Fenn, T., Pozharski, E., Wilson, M. A., Petsko, G. A., Karplus, M., Hubner, C. G., and Kern, D. (2007) Intrinsic motions along an enzymatic reaction trajectory. *Nature 450*, 838−844.

(8) Loria, J. P., Berlow, R. B., and Watt, E. D. (2008) Characterization of enzyme motions by solution NMR relaxation dispersion. *Acc. Chem. Res. 41*, 214−221.

(9) Ghanem, M., Li, L., Wing, C., and Schramm, V. L. (2008) Altered thermodynamics from remote mutations altering human toward bovine purine nucleoside phosphorylase. *Biochemistry 47*, 2559−2564.

(10) Hilser, V. J. (2010) An Ensemble View of Allostery. *Science 327*, 653−654.

(11) Nagel, Z. D., and Klinman, J. P. (2006) Tunneling and dynamics in enzymatic hydride transfer. *Chem. Rev. 106*, 3095−3118.

(12) Bhabha, G., Lee, J., Ekiert, D. C., Gam, J., Wilson, I. A., Dyson, H. J., Benkovic, S. J., and Wright, P. E. (2011) A Dynamic Knockout Reveals That Conformational Fluctuations Influence the Chemical Step of Enzyme Catalysis. *Science 332*, 234−238.

(13) Loveridge, E. J., Behiry, E. M., Guo, J. N., and Allemann, R. K. (2012) Evidence that a 'dynamic knockout' in *Escherichia coli* dihydrofolate reductase does not affect the chemical step of catalysis. *Nat. Chem. 4*, 292−297.

(14) Sawaya, M. R., and Kraut, J. (1997) Loop and subdomain movements in the mechanism of *Escherichia coli* dihydrofolate reductase: Crystallographic evidence. *Biochemistry 36*, 586−603.

(15) Boehr, D. D., McElheny, D., Dyson, H. J., and Wright, P. E. (2010) Millisecond timescale fluctuations in dihydrofolate reductase are exquisitely sensitive to the bound ligands. *Proc. Natl. Acad. Sci. U.S.A. 107*, 1373−1378.

(16) Oyeyemi, O. A., Sours, K. M., Lee, T., Resing, K. A., Ahn, N. G., and Klinman, J. P. (2010) Temperature dependence of protein motions in a thermophilic dihydrofolate reductase and its relationship to catalytic efficiency. *Proc. Natl. Acad. Sci. U.S.A. 107*, 10074−10079.

(17) Oyeyemi, O. A., Sours, K. M., Lee, T., Kohen, A., Resing, K. A., Ahn, N. G., and Klinman, J. P. (2011) Comparative Hydrogen-Deuterium Exchange for a Mesophilic vs Thermophilic Dihydrofolate Reductase at 25 °C: Identification of a Single Active Site Region with Enhanced Flexibility in the Mesophilic Protein. *Biochemistry 50*, 8251−8260.

(18) Rajagopalan, P. T., Lutz, S., and Benkovic, S. J. (2002) Coupling interactions of distal residues enhance dihydrofolate reductase catalysis: Mutational effects on hydride transfer rates. *Biochemistry 41*, 12618−12628.

(19) Swanwick, R. S., Shrimpton, P. J., and Allemann, R. K. (2004) Pivotal Role of Gly 121 in Dihydrofolate Reductase from *Escherichia coli*: The Altered Structure of a Mutant Enzyme May Form the Basis of Its Diminished Catalytic Performance. *Biochemistry 43*, 4119−4127.

(20) Wang, L., Goodey, N. M., Benkovic, S. J., and Kohen, A. (2006) Coordinated effects of distal mutations on environmentally coupled tunneling in dihydrofolate reductase. *Proc. Natl. Acad. Sci. U.S.A. 103*, 15753−15758.

(21) Mauldin, R. V., and Lee, A. L. (2010) Nuclear Magnetic Resonance Study of the Role of M42 in the Solution Dynamics of *Escherichia coli* Dihydrofolate Reductase. *Biochemistry 49*, 1606−1615.
(22) Mauldin, R. V., Sapienza, P. J., Petit, C. M., and Lee, A. L. (2012) Structure and Dynamics of the G121V Dihydrofolate Reductase Mutant: Lessons from a Transition-State Inhibitor Complex. *PLoS One 7*, e33252.
(23) Carroll, M. J., Mauldin, R. V., Gromova, A. V., Singleton, S. F., Collins, E. J., and Lee, A. L. (2012) Evidence for dynamics in proteins as a mechanism for ligand dissociation. *Nat. Chem. Biol. 8*, 246−252.
(24) Watney, J. B., Agarwal, P. K., and Hammes-Schiffer, S. (2003) Effect of Mutation on Enzyme Motion in Dihydrofolate Reductase. *J. Am. Chem. Soc. 125*, 3745−3750.
(25) Wong, K. F., Selzer, T., Benkovic, S. J., and Hammes-Schiffer, S. (2005) Impact of distal mutations on the network of coupled motions correlated to hydride transfer in dihydrofolate reductase. *Proc. Natl. Acad. Sci. U.S.A. 102*, 6807−6812.
(26) Liu, H., and Warshel, A. (2007) The Catalytic Effect of Dihydrofolate Reductase and Its Mutants Is Determined by Reorganization Energies. *Biochemistry 46*, 6011−6025.
(27) Radkiewicz, J. L., and Brooks, C. L., III (2000) Protein Dynamics in Enzymatic Catalysis: Exploration of Dihydrofolate Reductase. *J. Am. Chem. Soc. 122*, 225−231.
(28) Rod, T. H., Radkiewicz, J. L., and Brooks, C. L., III (2003) Correlated motion and the effect of distal mutations in dihydrofolate reductase. *Proc. Natl. Acad. Sci. U.S.A. 100*, 6980−6985.
(29) Agarwal, P. K., Billeter, S. R., Rajagopalan, P. T. R., Benkovic, S. J., and Hammes-Schiffer, S. (2002) Network of coupled promoting motions in enzyme catalysis. *Proc. Natl. Acad. Sci. U.S.A. 99*, 2794−2799.
(30) Garcia-Viloca, M., Truhlar, D. G., and Gao, J. (2003) Reaction-Path Energetics and Kinetics of the Hydride Transfer Reaction Catalyzed by Dihydrofolate Reductase. *Biochemistry 42*, 13558−13575.
(31) Cui, Q., and Karplus, M. (2002) Promoting Modes and Demoting Modes in Enzyme-Catalyzed Proton Transfer Reactions: A Study of Models and Realistic Systems. *J. Phys. Chem. B 106*, 7927−7947.
(32) Kamath, G., Howell, E. E., and Agarwal, P. K. (2010) The tail wagging the dog: Insights into catalysis in R67 dihydrofolate reductase. *Biochemistry 49*, 9078−9088.
(33) Boekelheide, N., Salomon-Ferrer, R., and Miller, T. F. (2011) Dynamics and dissipation in enzyme catalysis. *Proc. Natl. Acad. Sci. U.S.A. 108*, 16159−16163.
(34) Doron, D., Major, D. T., Kohen, A., Thiel, W., and Wu, X. (2011) Hybrid Quantum and Classical Simulations of the Dihydrofolate Reductase Catalyzed Hydride Transfer Reaction on an Accurate Semi-Empirical Potential Energy Surface. *J. Chem. Theory Comput. 7*, 3420−3437.
(35) Doron, D., Kohen, A., and Major, D. T. (2012) Collective Reaction Coordinate for Hybrid Quantum and Molecular Mechanics Simulations: A Case Study of the Hydride Transfer in Dihydrofolate Reductase. *J. Chem. Theory Comput. 8*, 2484−2496.
(36) Engel, H., Doron, D., Kohen, A., and Major, D. T. (2012) Momentum Distribution as a Fingerprint of Quantum Delocalization in Enzymatic Reactions: Open-Chain Path-Integral Simulations of Model Systems and the Hydride Transfer in Dihydrofolate Reductase. *J. Chem. Theory Comput. 8*, 1223−1234.
(37) Dametto, M., Antoniou, D., and Schwartz, S. D. (2012) Barrier crossing in dihydrofolate reductase does not involve a rate-promoting vibration. *Mol. Phys. 110*, 531−536.
(38) Pu, J., Gao, J., and Truhlar, D. G. (2006) Multidimensional tunneling, recrossing, and the transmission coefficient for enzymatic reactions. *Chem. Rev. 106*, 3140−3169.
(39) Garcia-Viloca, M., Gao, J., Karplus, M., and Truhlar, D. G. (2004) How enzymes work: Analysis by modern rate theory and computer simulations. *Science 303*, 186−195.
(40) Olsson, M. H. M., Parson, W. W., and Warshel, A. (2006) Dynamical contributions to enzyme catalysis: Critical tests of a popular hypothesis. *Chem. Rev. 106*, 1737−1756.
(41) Miller, G. P., and Benkovic, S. J. (1998) *Chem. Biol. 5*, R105−R113.
(42) Rozovsky, S., and McDermott, A. E. (2001) The time scale of the catalytic loop motion in triosephosphate isomerase. *J. Mol. Biol. 310*, 259−270.
(43) Tsai, C. J., del Sol, A., and Nussinov, R. (2008) Allostery: Absence of a change in shape does not imply that allostery is not at play. *J. Mol. Biol. 378*, 1−11.
(44) Wolfenden, R., and Snider, M. J. (2001) The depth of chemical time and the power of enzymes as catalysts. *Acc. Chem. Res. 34*, 938−945.
(45) Gao, J., and Xia, X. (1992) A prior evaluation of aqueous polarization effects through Monte Carlo QM-MM simulations. *Science 258*, 631−635.
(46) Gao, J., Ma, S., Major, D. T., Nam, K., Pu, J., and Truhlar, D. G. (2006) Mechanisms and free energies of enzymatic reactions. *Chem. Rev. 106*, 3188−3209.
(47) Gao, J., Wong, K.-Y., Major, D. T., Cembran, A., Song, L., Lin, Y.-L., Fan, Y., and Ma, S. (2009) Kinetic isotope effects from hybrid classical and quantum path integral computations. In *Quantum Tunnelling in Enzyme-Catalysed Reactions* (Allemann, R. K., Ed.) pp 105−131, Royal Society of Chemistry, Oxford, U.K.
(48) Gao, J. (1996) Hybrid Quantum Mechanical/Molecular Mechanical Simulations: An Alternative Avenue to Solvent Effects in Organic Chemistry. *Acc. Chem. Res. 29*, 298−305.
(49) Truhlar, D. G., Gao, J., Alhambra, C., Garcia-Viloca, M., Corchado, J., Sanchez, M. L., and Villa, J. (2002) The Incorporation of Quantum Effects in Enzyme Kinetics Modeling. *Acc. Chem. Res. 35*, 341−349.
(50) Senn, H. M., and Thiel, W. (2009) QM/MM methods for biomolecular systems. *Angew. Chem., Int. Ed. 48*, 1198−1229.
(51) Garcia-Viloca, M., Truhlar, D. G., and Gao, J. (2003) Importance of Substrate and Cofactor Polarization in the Active Site of Dihydrofolate Reductase. *J. Mol. Biol. 327*, 549−560.
(52) Pu, J., Ma, S., Gao, J., and Truhlar, D. G. (2005) Small Temperature Dependence of the Kinetic Isotope Effect for the Hydride Transfer Reaction Catalyzed by *Escherichia coli* Dihydrofolate Reductase. *J. Phys. Chem. B 109*, 8551−8556.
(53) Nagel, Z. D., Dong, M., Bahnson, B. J., and Klinman, J. P. (2011) Impaired protein conformational landscapes as revealed in anomalous Arrhenius prefactors. *Proc. Natl. Acad. Sci. U.S.A. 108*, 10520−10525.
(54) Karplus, M., and Kushick, J. N. (1981) Method for estimating the configurational entropy of macromolecules. *Macromolecules 14*, 325−332.
(55) Marlow, M. S., Dogan, J., Frederick, K. K., Valentine, K. G., and Wand, A. J. (2010) The role of conformational entropy in molecular recognition by calmodulin. *Nat. Chem. Biol. 6*, 352−358.
(56) Wand, A. J. (2012) The dark energy of proteins comes to light: Conformational entropy and its role in protein function revealed by NMR relaxation. *Curr. Opin. Struct. Biol.*, DOI: 10.1016/j.sbi.2012.11.005.
(57) Sikorski, R. S., Wang, L., Markham, K. A., Rajagopalan, P. T. R., Benkovic, S. J., and Kohen, A. (2004) Tunneling and Coupled Motion in the *Escherichia coli* Dihydrofolate Reductase Catalysis. *J. Am. Chem. Soc. 126*, 4778−4779.
(58) Stojkovic, V., Perissinotti, L. L., Willmer, D., Benkovic, S. J., and Kohen, A. (2012) Effects of the Donor-Acceptor Distance and Dynamics on Hydride Tunneling in the Dihydrofolate Reductase Catalyzed Reaction. *J. Am. Chem. Soc. 134*, 1738−1745.
(59) Roston, D., Cheatum, C. M., and Kohen, A. (2012) Hydrogen Donor-Acceptor Fluctuations from Kinetic Isotope Effects: A Phenomenological Model. *Biochemistry 51*, 6860−6870.
(60) Gao, J., and Truhlar, D. G. (2002) Quantum mechanical methods for enzyme kinetics. *Annu. Rev. Phys. Chem. 53*, 467−505.
(61) Knapp, M. J., Rickert, K., and Klinman, J. P. (2002) Temperature-dependent isotope effects in soybean lipoxygenase-1: Correlating hydrogen tunneling with protein dynamics. *J. Am. Chem. Soc. 124*, 3865−3874.
(62) Alhambra, C., Corchado, J., Sanchez, M. L., Garcia-Viloca, M., Gao, J., and Truhlar, D. G. (2001) Canonical Variational Theory for Enzyme Kinetics with the Protein Mean Force and Multidimensional

Quantum Mechanical Tunneling Dynamics. Theory and Application to Liver Alcohol Dehydrogenase. *J. Phys. Chem. B 105*, 11326−11340.
(63) Liu, H., and Warshel, A. (2007) Origin of the Temperature Dependence of Isotope Effects in Enzymatic Reactions: The Case of Dihydrofolate Reductase. *J. Phys. Chem. B 111*, 7852−7861.
(64) Major, D. T., and Gao, J. (2005) Implementation of the bisection sampling method in path integral simulations. *J. Mol. Graphics Modell. 24*, 121−127.
(65) Major, D. T., and Gao, J. (2007) An Integrated Path Integral and Free-Energy Perturbation-Umbrella Sampling Method for Computing Kinetic Isotope Effects of Chemical Reactions in Solution and in Enzymes. *J. Chem. Theory Comput. 3*, 949−960.
(66) Castillo, R., Andres, J., and Moliner, V. (1999) Catalytic Mechanism of Dihydrofolate Reductase Enzyme. A Combined Quantum-Mechanical/Molecular-Mechanical Characterization of Transition State Structure for the Hydride Transfer Step. *J. Am. Chem. Soc. 121*, 12140−12147.
(67) Agarwal, P. K., Billeter, S. R., and Hammes-Schiffer, S. (2002) Nuclear Quantum Effects and Enzyme Dynamics in Dihydrofolate Reductase Catalysis. *J. Phys. Chem. B 106*, 3283−3293.
(68) Cameron, C. E., and Benkovic, S. J. (1997) Evidence for a Functional Role of the Dynamics of Glycine-121 of *Escherichia coli* Dihydrofolate Reductase Obtained from Kinetic Analysis of a Site-Directed Mutant. *Biochemistry 36*, 15792.
(69) Venkitakrishnan, R. P., Zaborowski, E., McElheny, D., Benkovic, S. J., Dyson, H. J., and Wright, P. E. (2004) Conformational changes in the active site loops of dihydrofolate reductase during the catalytic cycle. *Biochemistry 43*, 16046−16055.
(70) Ohmae, E., Fukumizu, Y., Iwakura, M., and Gekko, K. (2005) Effects of mutation at methionine-42 of *Escherichia coli* dihydrofolate reductase on stability and function: Implication of hydrophobic interactions. *J. Biochem. 137*, 643−652.
(71) Thorpe, I. F., and Brooks, C. L., III (2005) Conformational Substates Modulate Hydride Transfer in Dihydrofolate Reductase. *J. Am. Chem. Soc. 127*, 12997−13006.
(72) Khavrutskii, I. V., Price, D. J., Lee, J., and Brooks, C. L., III (2007) Conformational change of the methionine 20 loop of *Escherichia coli* dihydrofolate reductase modulates pKa of the bound dihydrofolate. *Protein Sci. 16*, 1087−1100.
(73) Miyashita, O., Onuchic, J. N., and Wolynes, P. G. (2003) Nonlinear elasticity, proteinquakes, and the energy landscapes of functional transitions in proteins. *Proc. Natl. Acad. Sci. U.S.A. 100*, 12570−12575.
(74) del Sol, A., Tsai, C. J., Ma, B. Y., and Nussinov, R. (2009) The Origin of Allosteric Functional Modulation: Multiple Pre-existing Pathways. *Structure 17*, 1042−1050.
(75) Masterson, L. R., Shi, L., Metcalfe, E., Gao, J., Taylor, S. S., and Veglia, G. (2011) Dynamically committed, uncommitted, and quenched states encoded in protein kinase A revealed by NMR spectroscopy. *Proc. Natl. Acad. Sci. U.S.A. 108*, 6969−6974.
(76) Monod, J., Wyman, J., and Changeux, J. P. (1965) On the Nature of Allosteric Transitions: A Plausible Model. *J. Mol. Biol. 12*, 88−118.
(77) Koshland, D. E., Jr., Nemethy, G., and Filmer, D. (1966) Comparison of experimental binding data and theoretical models in proteins containing subunits. *Biochemistry 5*, 365−385.
(78) Gao, J., Wong, K.-Y., and Major, D. T. (2008) Combined QM/MM and path integral simulations of kinetic isotope effects in the proton transfer reaction between nitroethane and acetate ion in water. *J. Comput. Chem. 29*, 514−522.
(79) Major, D. T., Heroux, A., Orville, A. M., Valley, M. P., Fitzpatrick, P. F., and Gao, J. (2009) Differential quantum tunneling contributions in nitroalkane oxidase catalyzed and the uncatalyzed proton transfer reaction. *Proc. Natl. Acad. Sci. U.S.A. 106*, 20736−20739.
(80) Voth, G. A., Chandler, D., and Miller, W. H. (1989) Rigorous formulation of quantum transition state theory and its dynamical corrections. *J. Chem. Phys. 91*, 7749−7760.
(81) Voth, G. A. (1993) Feynman path integral formulation of quantum mechanical transition-state theory. *J. Phys. Chem. 97*, 8365−8377.
(82) Messina, M., Schenter, G. K., and Garrett, B. C. (1993) Centroid-density, quantum rate theory: Variational optimization of the dividing surface. *J. Chem. Phys. 98*, 8525−8536.
(83) Grote, R. F., and Hynes, J. T. (1980) The stable states picture of chemical reactions. II. Rate constants for condensed and gas phase reaction models. *J. Chem. Phys. 73*, 2715−2732.
(84) Feynman, R. P., and Hibbs, A. R. (1965) *Quantum Mechanics and Path Integrals*, McGraw-Hill, New York.
(85) Feynman, R. P., and Kleinert, H. (1986) Effective classical partition functions. *Phys. Rev. A 34*, 5080.
(86) Sprik, M., Klein, M. L., and Chandler, D. (1985) Staging: A sampling technique for the Monte Carlo evaluation of path integrals. *Phys. Rev. B 31*, 4234−4244.
(87) Hwang, J. K., and Warshel, A. (1993) A quantized classical path approach for calculations of quantum mechanical rate constants. *J. Phys. Chem. 97*, 10053−10058.
(88) Hwang, J.-K., and Warshel, A. (1996) How Important Are Quantum Mechanical Nuclear Motions in Enzyme Catalysis? *J. Am. Chem. Soc. 118*, 11745−11751.
(89) Hinsen, K., and Roux, B. (1997) Potential of mean force and reaction rates for proton transfer in acetylacetone. *J. Chem. Phys. 106*, 3567−3577.
(90) Lin, Y.-l., and Gao, J. (2011) Kinetic Isotope Effects of L-Dopa Decarboxylase. *J. Am. Chem. Soc. 133*, 4398−4403.
(91) Gao, J. (1995) Methods and applications of combined quantum mechanical and molecular mechanical potentials. In *Reviews in Computational Chemistry* (Lipkowitz, K. B., and Boyd, D. B., Eds.) pp 119−185, VCH, New York.
(92) Dewar, M. J. S., Zoebisch, E. G., Healy, E. F., and Stewart, J. J. P. (1985) Development and use of quantum mechanical molecular models. 76. AM1: A new general purpose quantum mechanical molecular model. *J. Am. Chem. Soc. 107*, 3902−3909.